TWELFTH EUROPEAN ROTORCRAFT FORUM

Paper No. 62

STUDY OF BENDING-TORSION FLUTTER OF A WIND TURBINE

Keiji Kawachi, Akira Azuma and Isao Watanabe

Institute of Interdisciplinary Research
Faculty of Engineering, The University of Tokyo
Tokyo, Japan

September 22—25, 1986

Garmisch-Partenkirchen
Federal Republic of Germany

Deutsche Gesellschaft für Luft- und Raumfahrt e. V. (DGLR)
Godesberger Allee 70, D-5300 Bonn 2, F.R.G.

STUDY OF BENDING-TORSION FLUTTER OF A WIND TURBINE

Keiji KAWACHI, Akira AZUMA and Isao WATANABE
Institute of Interdisciplinary Research
Faculty of Engineering, The University of Tokyo
Tokyo, Japan

ABSTRACT

An experimental study of the bending and torsion flutter of a propeller-type wind turbine was conducted by using a dynamically simulated model in the wind tunnel. It is confirmed from the wind tunnel test that the rotor is far apart from any flutter boundary in usual operational range.

In order to make clear a safety margin for the flutter boundary, an additional test was conducted for a modified rotor, the blade center-of-mass of which was shifted backward extremely by attaching a pair of mass to the tip of the respective blades. Thus, it made success to occur the bending and torsion flutter at a some operational condition.

The analytical study is also performed in order to develop a reliable method to estimate the onset of the flutter. The calculation using the Local Circulation Method (LCM) showed the reasonable agreement between the experiment and the theory.

1. Nomenclature

a	nondimensional position of elastic axis based on the half chord
b	half chord length
$C(k)$	Theodorsen function
$C_\ell(\alpha)$	lift coefficient
EI_y, EI_z, EI_{yz}	bending rigidities
e_{Ay}, e_{Az}	position of center of surface
e_y	distance between feathering axis and elastic axis
$\bar{e}_y$, $\bar{e}_z$	position of gravity center of blade section
GJ	torsional rigidity
g	gravity acceleration
h	normal displacement of a blade element, positive downward
$\bar{I}_x$, $\bar{I}_y$, $\bar{I}_z$, $\bar{I}_{yz}$	moments of inertia per unit length
i	inclination angle of tip-path-plane with respect to the general flow
k_A	radius of gyration

L_y, L_z	aerodynamic forces along y and z axes respectively
ℓ	lift acting on a blade element = $\ell_1+\ell_2$
ℓ_1	apparent mass component of the lift ℓ
ℓ_2	circulatory component of the lift ℓ
M_x	aerodynamic moment about x axis
m	blade mass per unit span or moment acting on a blade element = $m_1 + m_2$
m_1	apparent mass component of the moment m
m_2	circulatory component of the moment m
q	amplitude of mode
R	rotor radius
r	radius position of rotor blade
S(k)	Sears function
T	spanwise tension
U	stationary inflow velocity = $\sqrt{\bar{U}_T^2+\bar{U}_P^2}$
U_T	tangential component of the inflow velocity
$\bar{U}_T$	stationary component of U_T
U_P	normal component of the inflow velocity
$\bar{U}_P$	stationary component of U_P
u_c, v_c, w_c	displacement of elastic axis
V	wind velocity
v^j	induced velocity generated by the preceding j-th blade
Δv	induced velocity generated by the blade under consideration
x	nondimensional distance = r/R
α	angle of attack of a blade element = $\theta - \phi$
α_G	angle of attack caused by the induced velocity = $-(\sum_j v^j+\Delta v)/U$
β_p	preconing angle
θ	feathering angle
μ	advance ratio = $V\cos i/R\Omega$
ρ	air density
ϕ	stationary inflow angle = $\tan^{-1}(-\bar{U}_P/\bar{U}_T)$
ϕ_c	torsional axis
ψ	azimuth angle = Ωt
ω	frequency of natural vibration
$\dot{(\ )}$	time derivative = (d/dt)
$(\ )'$	spanwise derivative = (d/dr)
$\bar{(\ )}$	nondimensional value or mean value
$\hat{(\ )}$	mode of natural vibration

2. Introduction

It has been paid attention to the classical flutter, coupled vibration of bending and torsional motions, of rotary wings as well as fixed wings in many years. Since the respective blade of rotary wing is operated in the field of large centrifugal force and of strong downwash left by the preceding blades, more sophisticated analysis is required than that of fixed wings.

The linear perturbation method was proposed by Feingold[1] assuming the uniform induced velocity distribution over the rotor disc. The Floquet's theorem[2)-3)] was applied to extend the capability of the calculation to the rotor operating in an inclined flow. In order to take the non-uniform induced velocity distribution into the calculation, then the vortex theory[4)-5)] was proposed to the analyses of the flutter. However, the assumption of the uniform induced velocity distribution sometimes causes the inaccurate results, and also the vortex theory usually requires much computational time.

Furthermore, there are few experimental studies on the model rotor having dynamically simulated blades in the wind tunnel.

A propeller type wind turbine, the diameter of which is 7m, was recently developed in Japan.[6)] This wind turbine is set in the agricultural area to support the heat energy to the crops. In order to make clear the safety margine for the flutter boundary of this wind turbine, a dynamically simulated model was designed, and tested in the wind tunnel.

An analytical method to estimate the onset of the flutter of the wind turbine has been investigated by using the LCM,[7)] in which fully coupled elastic equations of motion of a turbine blade were combined with the calculation of the dynamic airloading acting on the deformed blade. The capability of this analytical method was examined by the comparison with the experimental results.

3. Model Rotor

The dimension of the model rotor shown in Fig. 1 is given in Table 1. This model rotor was designed to simulate the dynamic characteristics as well as the geometrical configuration of the real rotor.

Large efforts were spent to produce the model rotor to satisfy the similarity rule of the nondimensional parameters as shown in Appendix. The control of the mass and rigidity distributions along the blade span requires very sophisticated design procedure. The final configurations of the blade is as follows:

The I shaped beam, which is made of aluminium, and located at 40% chord at any blade section, is designed to support all components of the rigidity of the blade. The surface of the blade is, then, covered by a thin scotch tape, with the slits on it at a few particular spanwise positions to prevent the increase of the torsional rigidity.

Fig. 2 shows the distributions of the blade mass and the all components of rigidity in comparison with those of the real rotor. It is observed that the simulation was performed to be conservative for any critical vibration of the turbine.

However, it is, from the actual beam design, impossible to satisfy the simularity rule for all nondimensional parameters of the rigidity in this simple blade configuration. Specifically, the torsional moment of inertia is extremely different from that of the real rotor. The undamped natural frequency of the torsional vibration is, therefore, adjusted by a mass balance attached to the respective blade tip (r/R = 0.978). The chord-wise position of the mass balance is movable to alter the above natural frequency as shown in Fig. 3

The Reynolds number is simulated approximately whereas the nondimensional gravity force ($g/R\Omega^2$) is out of the simulation because the latter is not important to the flutter study.

4. The Analytical Method

The aerodynamic force and moment are calculated by the LCM concerning unsteady aerodynamic efforts as follows:

The tangential and normal components of the inflow velocity with respect to a blade element are given respectively by

$$\left.\begin{aligned} U_T &= R\Omega(x+\mu\sin\psi)+(\sum_j v^j+\Delta v)\sin\phi+\dot{v}_c \\ U_P &= -R\Omega\mu\tan i+(\sum_j v^j+\Delta v)\cos\phi-\dot{w}_c-R\Omega w_c'\mu\cos\psi \end{aligned}\right\} \quad (1)$$

where

$$\left.\begin{aligned} \phi &= \tan^{-1}(-U_P/U_T) \\ U_P &= -R\Omega\mu\tan i-\dot{w}_c-R\Omega w_c'\mu\cos\psi \\ U_T &= R\Omega(x+\mu\sin\psi)+\dot{v}_c \end{aligned}\right\} \quad (2)$$

Then the lift and moment of the blade element can be given by

$$\left.\begin{aligned} \ell &= \ell_1+\ell_2 \\ m &= m_1+m_2 \end{aligned}\right\} \quad (3)$$

where $(\ )_1$ and $(\ )_2$ show the apparent mass components and circulatory components respectively, and are, hence, given by

$$\left.\begin{aligned} \ell_1 &= \rho\pi b^2(\ddot{h}+U\dot{\alpha}-ab\ddot{\alpha}) \\ m_1 &= \rho\pi b^3\{a\ddot{h}-U(\tfrac{1}{2}-a)\dot{\alpha}-b(\tfrac{1}{8}+a^2)\ddot{\alpha}\} \\ \ell_2 &= \rho U^2 b[C(k)C_\ell(\alpha)+S(k)C_\ell(\alpha_G)] \\ m_2 &= b(a+\tfrac{1}{2})\ell_2 \end{aligned}\right\} \quad (4)$$

$$
\left.
\begin{aligned}
U &= \sqrt{\bar{U}_T^{\,2} + \bar{U}_P^{\,2}} \\
\dot{h} &= \{-\dot{w}_c - R\Omega w_c' \beta \cos\psi\}\cos\phi + \dot{v}_c \sin\phi \\
\alpha &= \theta - \phi = \theta - \tan^{-1}(-\bar{U}_P / \bar{U}_T) \\
\alpha_G &= -(\sum_j v^j + \Delta v)/U
\end{aligned}
\right\} \qquad (5)
$$

and where the induced velocity mainly generated by the trailing vortices, $\sum_j v^j + \Delta v$, has been regarded as if there is a vertical gust for the blade element. The effect of shed vortices on the lift and moment has been represented by the Theodorsen and Sears functions.

The equations of motion of the blade elasticity are given in Appendix, for the displacements parpendicular to the rotational plane, w_c, the displacement parallel to the rotational plane, v_c, and the torsional displacements, ϕ_c. These equations are solved simultaneously by the mode expansion method,

$$
\{w_c(r,t), v_c(r,t), \phi_c(r,t)\}^T = \sum_{j=1}^{j} \{\hat{w}_j(r), \hat{v}_j(r), \hat{\phi}_j(t)\}^T q_j(t) \qquad (6)
$$

The frequencies and the modes of the natural vibration are analyzed by using Holzer-Myklestadt method, and are shown in Fig. 4(a) and 4(b) for the blade with and without tip weight, respectively.

By using these natural frequencies and modes, the ordinary differential equations of the second order are derived from the equations of motion (A4-A6). These equations are numerically calculated to be coupled with aerodynamic and inertial forces and moments, given by the LCM.

5. The Results and Discussion

In order to make clear the safety margine of the flutter, the experimental test under the normal working state was firstly conducted by using the model rotor without any tip weight.

The results of the performance are shown in Fig. 5 in comparison with the analyses. The aerodynamic data of the two-dimensional airfoil section used in this analyses, is shown in Fig. 6. It is observed from Fig. 5 that the reasonable correlation is obtained between analyses and experiments. This indicates that the analytical method and the measurement technique concerning the aerodynamic force and moment are well established and reliable.

The chordwise center of gravity of the blade was, then, shifted by the tip weight, and the additional experiment was conducted.

When the natural frequency of the torsional vibration is simulated to the actual blade, the model blade is very stable far from the flutter boundary.

The bending-torsion flutter successfully occurred at an operational condition of a rotational speed of Ω =45.03 rad./sec and of wind velocity of V = 8m/s.

This onset of the flutter is well predicted by the present analytical method, as shown in Fig. 7. The time history of the onset of the flutter is also shown in Fig. 8.

6. Conclusions

The study on the bending-torsion flutter is conducted by using a dynamically simulated model rotor. The analytical method to predict the flutter onset is also developed by using the LCM fully coupled with the blade elastic deformation of the three degree of freedom. The flutter of the model rotor occurred at a some operational condition with the tip weight shifted extremely backward. This flutter onset is well predicted by the present analytical method. In addition, the reasonable agreement is obtained between the theory and the experiment concerning the performance of the wind turbine at many operating conditions including the blade stall.

REFERENCES

1. A. M. Feingold — Theory of Mechanical Oscillations of Rotors with Two Hinged Blades. NACA Wartime Report ARR No. 3I13, (1943)

2. D. A. Peters, K. Hohenemser — Application of the Floquet Transition Martrix to Problems of Lifting Rotor Stability. J. of the AHS, Vol. 16, No. 2, pp. 25-33, (1971)

3. P. Friedmann, C. E. Hammond — Efficient Numerical Treatment of Periodic Systems with Application to Stability Problems. International J. for Numerical Methods in Engineering, Vol. 11, pp. 1117-1136, (1977)

4. C. J. Astill, C. F. Niebanch — Prediction of Rotor Instability at High Forward Speeds. Vol. II, Classical Flutter. USAAVLABS, TR 68-18B, AD 683861, (1969)

5. K. W. Shipman, E. R. Wood — A Two-Dimensional Theory for Rotor Blade Flutter in Forward Flight. J. of Aircraft, Vol. 8, No. 12, pp. 1008-1015, (1971)

6. Y. Ishida, et al. Experimental Study on the Optimal Efficiency Design of Wind Turbine. NAL TR 698, (1982)

7. A. Azuma, K. Kawachi, T. Hayashi, A. Ito Application of the Local Circulation Method to the Flutter Analysis of Rotary Wings. 8th European Rotorcraft Forum Paper No. 3. 12. (1982)

Appendix Simularity Rule

According to the x-y-z coordinate system shown in Fig. A-1, the equation of the blade elasticity is given by

$$\left.\begin{aligned}&[EI_{yz}v_c''+EI_y w_c'']''-(Tw_c')'+m(\ddot{w}_c+\bar{e}_y\ddot{\phi}_c)\\&+[\bar{I}_y(-\ddot{w}_c'+\Omega^2 w_c')+\bar{I}_{yz}(-\ddot{v}_c'+\Omega^2 v_c')-m\bar{e}_y r\Omega^2\phi_c-m\bar{e}_z(-\ddot{u}_c+\Omega^2 u_c)]'\\&=L_z-mr\Omega^2\beta_p+[m\bar{e}_z r\Omega^2+2\bar{I}_y\Omega\dot{\phi}_c-2m\bar{e}_z\Omega\dot{v}_c]'+mg\beta_p\sin\psi\end{aligned}\right\}\quad(A-1)$$

$$\left.\begin{aligned}&[EI_z v_c''+EI_{yz}w_c'']''-(Tv_c')'+m[\ddot{v}_c-\Omega^2 v_c-\bar{e}_z(\ddot{\phi}-\Omega^2\phi_c)]\\&-[\bar{I}_z(\ddot{v}_c-2\Omega^2 v_c')+\bar{I}_{yz}(\ddot{w}_c'-2\Omega^2 w_c')-m\bar{e}_y(\ddot{u}_c-\Omega^2 u_c)-m\bar{e}_z r\Omega^2\phi_c]'\\&=L_y-me_y\Omega^2+[m\bar{e}_y r\Omega^2+2\bar{I}_{yz}\Omega\dot{\phi}_c-2m\bar{e}_y\Omega\dot{v}_c]'+mg\cos\psi\end{aligned}\right\}\quad(A-2)$$

$$\left.\begin{aligned}&-[(GJ+Tk_A^2)\phi_c']'+Te_{Az}v_c''-Te_{Ay}w_c''+\bar{I}_x\ddot{\phi}_c+(\bar{I}_z-\bar{I}_y)\Omega^2\phi_c\\&+m[\bar{e}_y(\ddot{w}_c+r\Omega^2 w_c')+\bar{e}_z(-\ddot{v}_c+\Omega^2 v_c-r\Omega^2 v_c')]\\&=M_x-\bar{I}_{yz}\Omega^2+m\bar{e}_z e_y\Omega^2+2\Omega(\bar{I}_y\dot{w}_c'+\bar{I}_{yz}\dot{v}_c')-2m\bar{e}_z\Omega\dot{u}_c\\&-m\bar{e}_y r\Omega^2\beta_p\end{aligned}\right\}\quad(A-3)$$

These equations are *nondimensionalized as follows:*

$$\left.\begin{aligned}&[\bar{\bar{E}}\bar{\bar{I}}_{yz}\bar{v}_c''+\bar{\bar{E}}\bar{\bar{I}}_y\bar{w}_c'']''-(\bar{\bar{T}}\bar{w}_c')'+\bar{m}(\ddot{\bar{w}}_c+\bar{\bar{e}}_y\ddot{\phi}_c)\\&+[\bar{\bar{I}}_y(-\ddot{\bar{w}}_c'+\bar{w}_c')+\bar{\bar{I}}_{yz}(-\ddot{\bar{v}}_c'+\bar{v}_c')-\bar{\bar{m}}\bar{\bar{e}}_y\bar{r}\phi_c-\bar{\bar{m}}\bar{\bar{e}}_z(-\ddot{\bar{u}}_c+\bar{u}_c)]'\\&=\bar{L}_z-\bar{\bar{m}}\bar{\bar{r}}\beta_p+[\bar{\bar{m}}\bar{\bar{e}}_z\bar{r}+2\bar{\bar{I}}_y\dot{\phi}_c-2\bar{\bar{m}}\bar{\bar{e}}_z\dot{\bar{v}}_c]'+\bar{\bar{m}}\bar{\bar{g}}\beta_p\sin\psi\end{aligned}\right\}\quad(A-4)$$

$$\left.\begin{aligned}&[\bar{\bar{E}}\bar{\bar{I}}_z\bar{v}_c''+\bar{\bar{E}}\bar{\bar{I}}_{yz}\bar{w}_c'']''-(\bar{\bar{T}}\bar{v}_c')'+\bar{\bar{m}}[\ddot{\bar{v}}_c-\bar{v}_c-\bar{\bar{e}}_z(\ddot{\phi}-\phi_c)]\\&-[\bar{\bar{I}}_z(\ddot{\bar{v}}_c-2\bar{v}_c')+\bar{\bar{I}}_{yz}(\ddot{\bar{w}}_c'-2\bar{w}_c')-\bar{\bar{m}}\bar{\bar{e}}_y(\ddot{\bar{u}}_c-\bar{u}_c)-\bar{\bar{m}}\bar{\bar{e}}_z\bar{r}\phi_c]'\\&=\bar{\bar{L}}_y-\bar{\bar{m}}\bar{\bar{e}}_y+[\bar{\bar{m}}\bar{\bar{e}}_y\bar{r}+2\bar{\bar{I}}_{yz}\dot{\phi}_c-2\bar{\bar{m}}\bar{\bar{e}}_y\dot{\bar{v}}_c]'+\bar{\bar{m}}\bar{\bar{g}}\cos\psi\end{aligned}\right\}\quad(A-5)$$

$$
\begin{aligned}
&-[(\bar{\bar{G}}\bar{\bar{J}}+\bar{\bar{T}}\bar{\bar{k}}_A^2)\phi']'+\bar{\bar{T}}\bar{\bar{e}}_{Az}\bar{v}_c''-\bar{\bar{T}}\bar{\bar{e}}_{Ay}\bar{w}_c''+\bar{\bar{\bar{I}}}_x\ddot{\phi}+(\bar{\bar{\bar{I}}}_z-\bar{\bar{\bar{I}}}_y)\phi_c \\
&+\bar{m}[\bar{\bar{e}}_y(\ddot{\bar{w}}_c+\bar{\bar{r}}\bar{\bar{w}}_c')+\bar{\bar{e}}_z(-\ddot{\bar{v}}_c+v_c-\bar{\bar{r}}\bar{\bar{v}}_c')] \\
&=\bar{M}_x-\bar{\bar{\bar{I}}}_{yz}+\bar{m}\bar{\bar{e}}_z\hat{e}_y+2(\bar{\bar{\bar{I}}}_y\dot{\bar{w}}_c'+\bar{\bar{\bar{I}}}_{yz}\dot{\bar{v}}_c') \quad 2\bar{m}\bar{\bar{e}}_z\dot{u}_c \\
&-\bar{m}\bar{\bar{e}}_y\bar{r}\beta_p
\end{aligned}
\qquad \text{(A-6)}
$$

where

$$
\begin{aligned}
\bar{\bar{E}}\bar{\bar{I}}_y &= EI_y/m_bR^3\Omega^2 \\
\bar{\bar{E}}\bar{\bar{I}}_{yz} &= EI_{yz}/m_bR^3\Omega^2 \\
\bar{\bar{E}}\bar{\bar{I}}_z &= EI_z/m_bR^3\Omega^2 \\
\bar{e}_{Ay} &= \bar{e}_{Ay}/R \\
\bar{e}_{Az} &= \bar{e}_{Az}/R \\
\bar{\bar{G}}\bar{\bar{J}} &= GJ/m_bR^3\Omega^2 \\
\bar{m} &= m/(m_b/R) \\
\bar{w}_c &= w_c/R \\
\bar{T} &= T/m_bR\Omega^2 \\
\bar{k}_A &= k_A/R \\
\bar{v}_c &= v_c/R \\
\bar{\bar{\bar{I}}}_x &= \bar{I}_x/m_bR \\
\bar{\bar{\bar{I}}}_y &= \bar{I}_y/m_bR \\
\bar{\bar{\bar{I}}}_{yz} &= \bar{I}_{yz}/m_bR
\end{aligned}
\qquad \text{(A-7)}
$$

$$\bar{\bar{I}}_z = \bar{I}_z/m_b R$$

$$\bar{\bar{e}}_y = \bar{e}_y/R$$

$$\bar{\bar{e}}_z = \bar{e}_z/R$$

$$\bar{r} = r/R$$

$$\hat{e}_y = e_y/R$$

$$\bar{M}_x = M_x/m_b R\Omega^2$$

$$\bar{\bar{L}}_z = L_z/m_b \Omega^2$$

$$\bar{L}_y = L_y/m_b \Omega^2$$

$$\bar{g} = g/R\Omega^2$$

$$(\,)' = R\frac{d}{dr}(\,)$$

$$(\dot{}) = \frac{1}{\Omega}\frac{d}{dt}(\,)$$

(A-7)

Therefore, if the two different blades has the same value of the nondimensional parameter given by eq. (A-7), these blades have the same dynamic behaviours.

Table 1. Dimension of Model Rotor

Items	Unit	Value
Rotor radius	m	0.70
Number of blades		2
Mean chord	m	0.0528
Taper ratio		0.315
Twist angle	deg.	29.5
Rotational speed	rad./sec	73.3
Flapwise first bending natural frequency	Hz	21.8
First torsional natural frequency	Hz	25.6
Airfoil section		NACA 4418

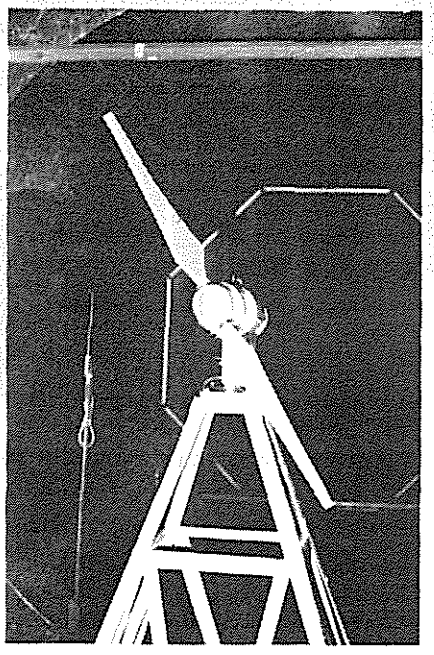

Figure 1. Model rotor

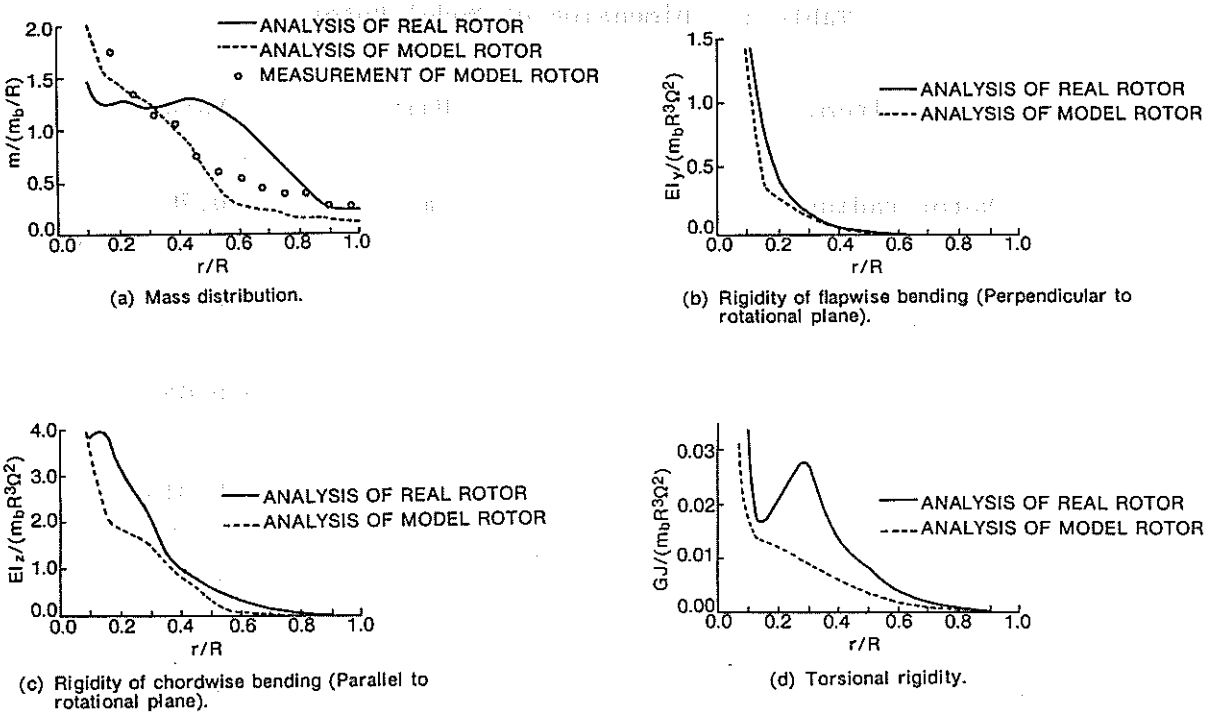

Figure 2. Distributions of non-dimensional mass and rigidity.

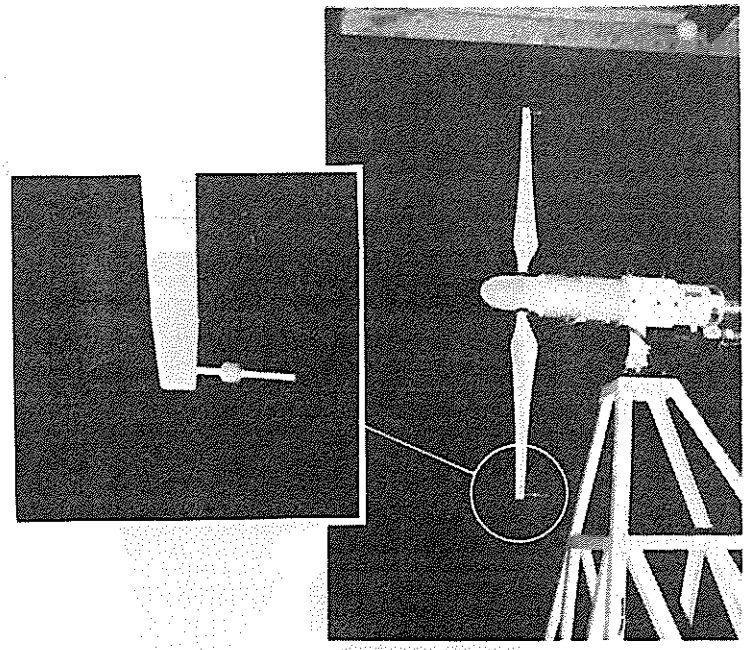

Figure 3. Mass balance at the blade tip.

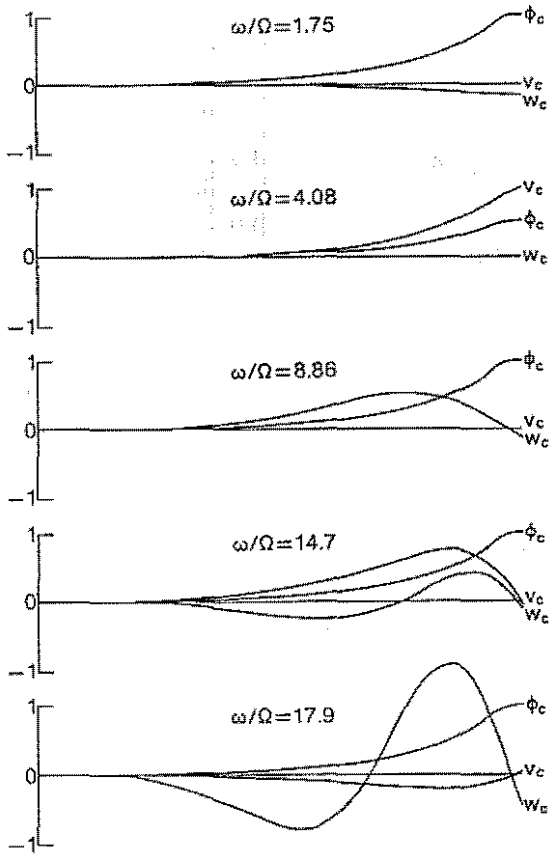

Figure 4(a). Natural frequency and mode with tip weight.
Ω=52.36 rad./s

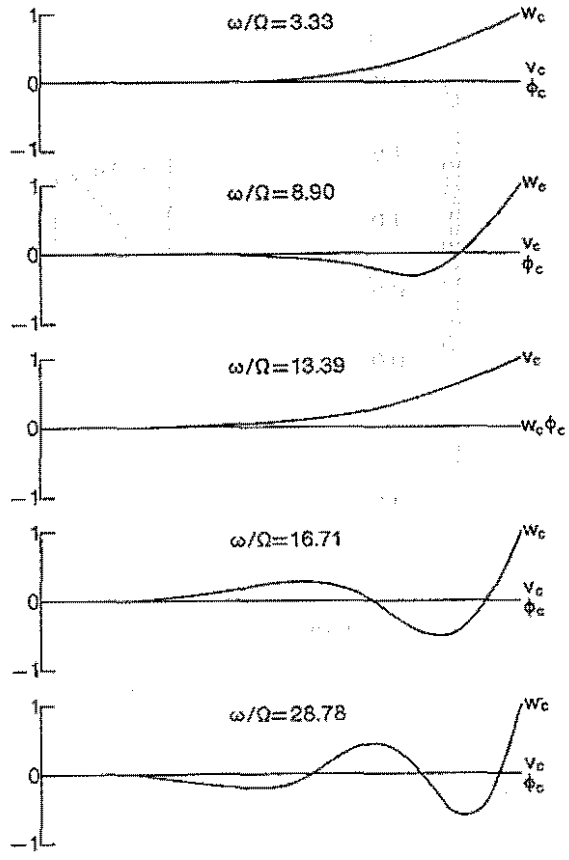

Figure 4(b). Natural frequency and mode without tip weight.
Ω=52.36 rad./s

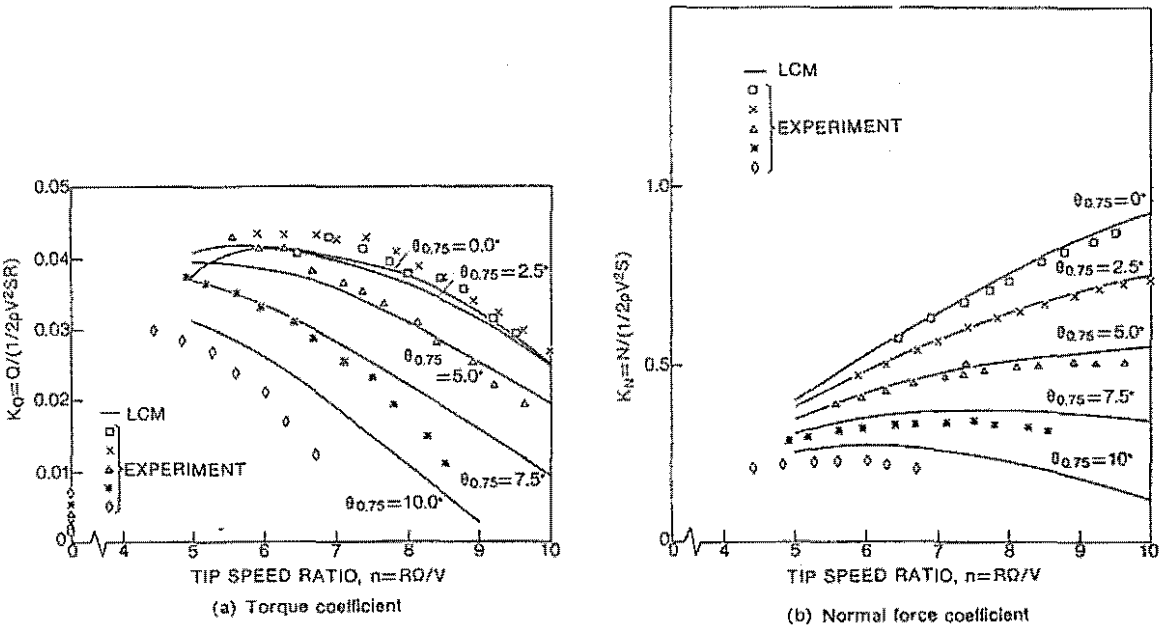

Figure 5. Aerodynamic performance (V=5m/s).

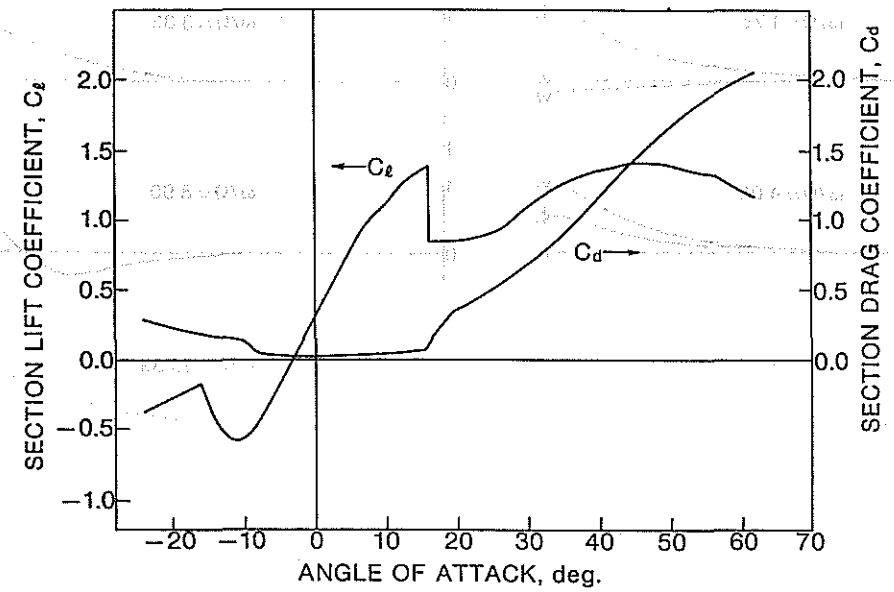

Figure 6. Aerodynamic characteristics of blade section.

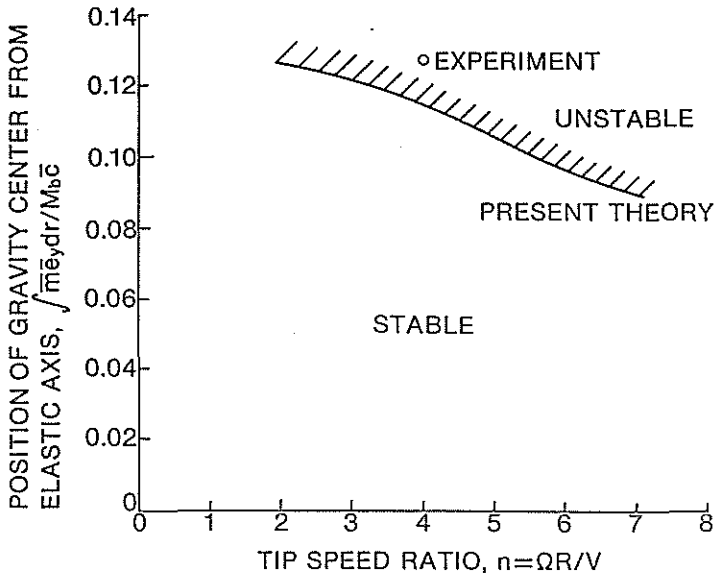

Figure 7. Measured and analytical results of flutter boundary.

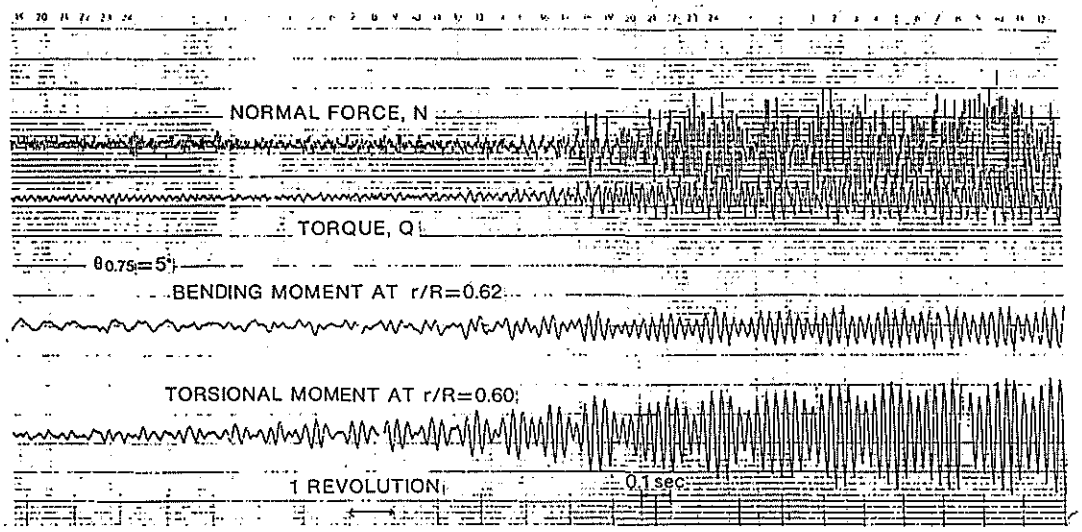

Figure 8. Time history of bending and torsion flutter.

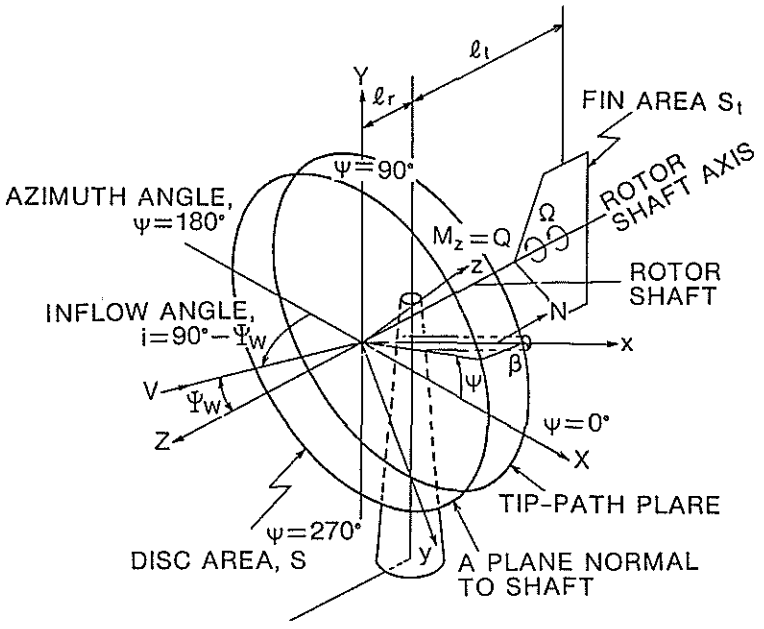

Figure A.1. Wind turbine and coordinate system.